J. Ocean Univ. China (Oceanic and Coastal Sea Research)
DOI 10.1007/s11802-017-3322-8
ISSN 1672-5182, 2017 16 (4): 602-608
http://www.ouc.edu.cn/xbywb/
E-mail:xbywb@ouc.edu.cn

Numerical Modeling of Floating Oil Boom Motions in Wave-Current Coupling Conditions

SHI Yang[1)], LI Shaowu[1), *], ZHANG Huaqin[2)], PENG Shitao[2)], CHEN Hanbao[2)], ZHOU Ran[2)], and MAO Tianyu[2)]

1) *State Key Laboratory of Hydraulic Engineering Simulation and Safety*, *Tianjin University*, *Tianjin* 300072, *P. R. China*
2) *Tianjin Research Institute for Water Transport Engineering*, *Ministry of Transport*, *Tianjin* 300456, *P. R. China*

(Received January 3, 2017; revised May 19, 2017; accepted June 5, 2017)

Abstract Containment booms are commonly used in collecting and containing spilled oil on the sea surface and in protecting specific sea areas against oil slick spreading. In the present study, a numerical model is proposed based on the N-S equations in a mesh frame. The proposed model tracks the outline of the floating boom in motion by using the fractional area/volume obstacle representation technique. The boom motion is then simulated by the technique of general moving object. The simulated results of the rigid oil boom motions are validated against the experimental results. Then, the failure mechanism of the boom is investigated through numerical experiments. Based on the numerical results, the effects of boom parameters and dynamic factors on the oil containment performance are also assessed.

Key words floating oil boom; hydrodynamic performance; CFD

1 Introduction

Floating oil booms are commonly used in collecting spilled oil and in preventing oil from spreading. Their ability to contain oil slick depends on their characteristics and on how they respond to the external dynamic environment. The major characteristics of floating boom include the effective depth of the draft, the effective freeboard height, and buoyancy/weight (B/W) ratio. External dynamic environmental factors include waves, currents, and winds. The failure modes of oil containment, such as submergence, splash-over, overturning, and drainage, are directly related to the dynamic performance of the floating oil boom, whereas others, such as critical accumulation and entrainment, are indirectly affected by the dynamic conditions.

Kim *et al*. (1998) conducted numerous experiments to investigate the seakeeping performance of a floating boom. They reported that booms with higher B/W ratio are more effective against the failure mode of oversplashing. Lee and Kang (1995) investigated the oil boom performance under waves and currents through laboratory experiments. They reported that the current's influence on the oil boom is determined by the ratio of the ballast weight and the dynamic pressure in front of the oil boom. Lee also observed that when wave steepness is relatively small, the seakeeping characteristics of oil boom behave well. Meanwhile, Castro *et al*. (2010) and Iglesias *et al*. (2010) investigate floating boom behavior by developing an artificial intelligence technique. They presented the design methods of the effective draft's significant value while considering the boom features under different current and wave conditions.

The majority of studies on the hydrodynamic performances of a floating oil boom are based on laboratory experiments or on numerical simulations with fixed boom (Goodman *et al*., 1996; Fang and Johnston, 2001a, b, c). However, such situations are far different from actual conditions. Very few studies are based on numerical analysis via movable floating boom. Amini *et al*. (2005) reported the numerical results of oil boom motion under the coupling interaction of hydraulic factors and structure, and reported that a flexible skirt can significantly affect the failure process of oil spill. By using the CFD model, Feng *et al*. (2011) simulated the oil contaminant process by developing a half-coupling model and then presenting an empirical relation between oil loss rate and wave steepness. Meanwhile, to model oil spill containment Yang and Liu (2013) proposed a modified multi-phase smoothed particle hydrodynamics method by using a boom that moves freely in the vertical direction and at a constant horizontal velocity.

The present study aims to establish a numerical platform for the simulation of the movable floating boom under wave-current coupling conditions. The oil containment

* Corresponding author. E-mail: lishaowu@tju.edu.cn

performances of the floating booms are also investigated.

2 Mathematical Formulas

2.1 Governing Equations

The mass conservation equation can be written as

$$\frac{\partial}{\partial x_i}(u_i A)=\frac{S}{\rho}, \tag{1}$$

where u_i denotes the fluid velocity components, A is the fractional area open to flow, and S is the mass source due to moving object.

The momentum conservation equations is given by

$$\frac{\partial u_i}{\partial t}+\frac{1}{V_F}u_j A\frac{\partial u_i}{\partial x_j}=-\frac{1}{\rho}\frac{\partial p}{\partial x_i}+G_i-\frac{1}{\rho V_F}\frac{\partial}{\partial x_j}\left(A\tau_{ij}\right)+\frac{S}{\rho V_F}\left(u_i-u_{io}\right), \tag{2}$$

where V_F denotes the fractional volume open to flow, p is the pressure, G_i is the body force components, u_{io} is the moving object velocity component, and τ_{ij} is the viscous shear stress tensor, which is defined as

$$\tau_{ij}=\mu\left(\frac{\partial u_i}{\partial u_j}+\frac{\partial u_j}{\partial u_i}\right). \tag{3}$$

At each time step, fluid volume fractions are updated for the temporal location and orientation of the oil boom by using the VOF method (Hirt and Nichols, 1981).

2.2 Turbulence Modeling

The two-equation k-ε model, which is adopted in this study for closure, is expressed as

$$\frac{\partial k_T}{\partial t}+\frac{1}{V_F}u_i A\frac{\partial k_T}{\partial x_i}=P_T+G_T+D_{k_T}+\varepsilon_T, \tag{4}$$

$$\frac{\partial \varepsilon_T}{\partial t}+\frac{1}{V_F}u_i A\frac{\partial \varepsilon_T}{\partial x_i}=\frac{C_1\varepsilon_T}{k_T}\left(P_T+C_3G_T\right)+D_\varepsilon-C_2\frac{\varepsilon_T}{k_T}, \tag{5}$$

where k_T denotes the turbulent kinetic energy, ε_T is the dissipation rate of turbulent kinetic energy, P_T is the turbulent kinetic energy production, G_T is the buoyancy production term, D_{kT} and D_ε are the turbulent diffusion terms, and C_1, C_2, and C_3 are the dimensionless parameters, with their default values being 1.44, 1.92, and 0.2, respectively.

2.3 General Moving Objects Model

In this study, we simulate the oil boom movement under wave–current coupling condition, by using the general moving object technique. Here we assumed that the oil boom is a rigid object and proceeded to simplify it as a particle whose mass is concentrated at the centroid and moves with 3 degrees of freedom (DOF) for a two-dimensional (2D) simulation. The motion of the floating boom is governed by the dynamic equations

$$F_G=M\frac{\mathrm{d}V_G}{\mathrm{d}t}, \tag{6}$$

$$T_G=I\frac{\mathrm{d}\omega}{\mathrm{d}t}+\omega\left(I\cdot\omega\right), \tag{7}$$

where F_G denotes the total load exerting on the centroid of the floating boom, T_G is the total torque of the floating boom in relation to the centroid, M is the floating boom mass, I is the floating boom's inertia moment tensor, and V_G and ω are the velocity and angular velocity tensor, respectively.

2.4 Simulation of Solid Boundary

Simulation of distorted geometric boundary is a severe problem encountered in using conventional FDM for the simulation of water wave and structure interaction. One major example, the zigzag boundary, can substantially influence the simulation accuracy around the solid boundary, especially for the case of a movable object. The problem was effectively solved by Hirt and Sicilian (1990) using the FAVOR technique. The FAVOR method takes the geometry effects of the model into account and incorporates the area fractions of the modeled structure into the governing equations. Fig.1 compares the floater of a floating boom described using the conventional FDM and the FAVOR method.

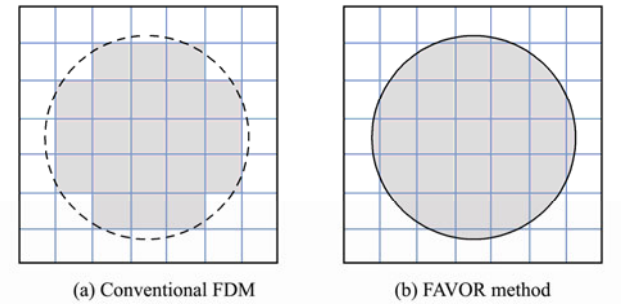

Fig.1 Comparison of the different approaches of boundary treatment.

3 Validation of the Numerical Model

3.1 Physical Experiment Setup

Here, we present a brief description of the experiment tests. Details of the experiment can be found in Shi *et al.* (2017). The experiments were carried out in the wave–current flume of the Tianjin Research Institute for Water Transport Engineering, Ministry of Transportation. The flume has a length of 45 m, a width of 0.5 m, and an initial water depth of 0.8 m. A piston-type wave maker was equipped on the right-hand side of the flume, and a wave absorber was placed at the opposite side of the flume. In the middle of the flume an oil floating boom consisting of a vertical skirt, a cylindrical floater, and a balance weight was placed. The floating boom was restricted in the longitudinal direction by two horizontally parallel mooring

lines, which were attached to the connection point of the floater and the skirt. This setup allowed the floating boom to move with three DOF under the action of combined current and wave. The parameters of the floating oil booms are listed in Table 1.

Table 1 Model boom parameters

Parameters	M1	M2	M3	M4	M5
Diameter of floater (m)	0.100	0.100	0.100	0.050	0.050
Length of skirt (m)	0.100	0.100	0.100	0.100	0.050
B/W ratio	7.830	4.700	3.360	3.430	3.430

3.2 Numerical Model Setup

By considering the computer load, the computational domain was set at 20 m long and 1 m high (Fig.2). The water depth was the same as that used in the physical test. The floating boom was located at the middle of the flume, and its boom parameters were the same as those in the physical model. Currents and waves were generated using velocity boundary at the right-side end, whereas the Sommerfeld boundary condition combined with artificial sponge layer was adopted for wave absorption at the downstream end of the flume (Jacobsen *et al*., 2012). The length of the relaxation zone was about 1.5 times the wavelength. A total of 90000 grids were employed in the computation with mesh size ranging from 0.005 m to 0.02 m. A fine mesh was adopted around the free surface and the floating boom to ensure high resolution. The wave and current conditions are summarized in Tables 2 and 3, respectively.

Table 2 Current characteristics

	V1	V2	V3	V4
Current velocity ($m\,s^{-1}$)	0.139	0.185	0.230	0.276

Table 3 Wave characteristics

	W1	W2	W3	W4	W5	W6	W7
Wave height (m)	0.04	0.04	0.06	0.06	0.06	0.08	0.08
Period (s)	1.3	2.2	1.2	1.7	2.2	1.2	2.2
Wave steepness	0.016	0.007	0.027	0.015	0.011	0.036	0.015

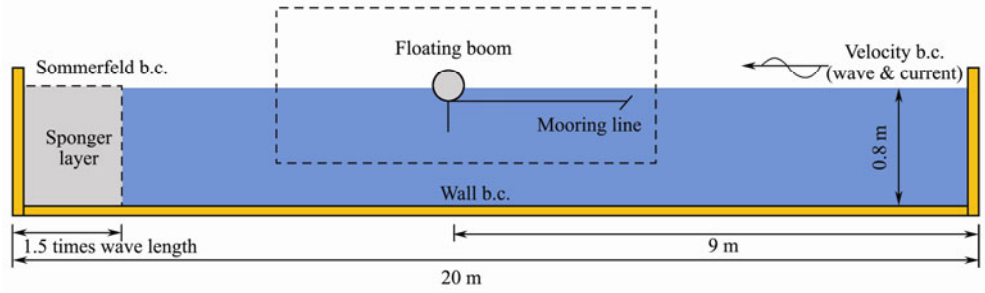

Fig.2 Sketch of the numerical setup.

3.3 Validation Results

For the numerical model verification, the case with wave height of 0.04 m, current velocity of 0.139 $m\,s^{-1}$, and wave period of 1.3 s was selected. Definitions of the heave, sway, and roll as well as the other related parameters, are shown in Fig.3, in which θ is positive in the clockwise direction, and Φ, h, D, F denote the values of the diameter of the floater, length of the skirt, the draft, and the freeboard, respectively.

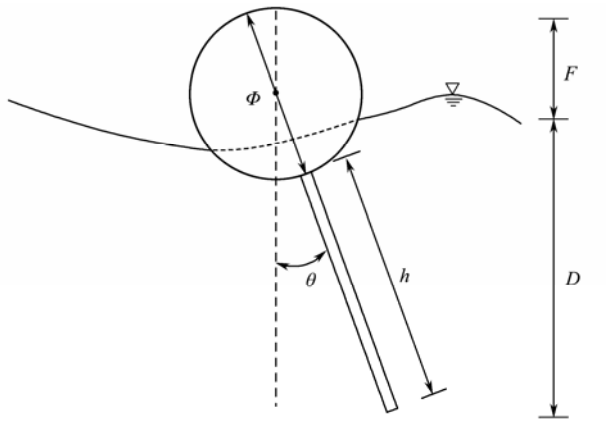

Fig.3 Schematic of the floating oil boom cross-section.

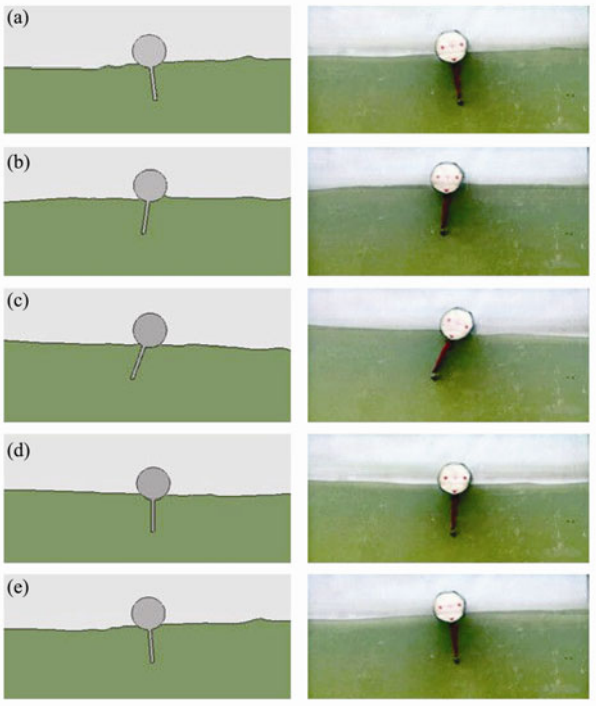

Fig.4 Floating boom poses and ambient water surface elevations for wave of H=0.04 m, T=1.3 s. a), $t=t_0$; b), $t=t_0+T/4$; c), $t=t_0+T/2$; d), $t=t_0+3T/4$; and e), $t=t_0+T$. Left, numerical calculations; Right, experimental photos.

Fig.4 shows the comparison between the modeled and experimental snapshots of the positions of the oil boom at various phases of the wave period, which are obtained by using the floating boom model M2. As can be seen, good consistency is obtained between the positions of the floating boom and the ambient water surface elevations. The floating boom first rotates clockwise as the wave crest comes from right, and then gains the maxima of vertical displacement at $t_0+T/4$ when the wave crest reaches the floating boom. When the wave crest passes through the floating boom, due to the effect of the inertia, the boom tends to rotate in the clockwise direction under the restriction of the mooring line. Maxima of the roll responses are gained at about $t_0+T/2$. Afterwards, the floating boom begins to rotate counterclockwise and returns to a nearly vertical pose at $t_0+3T/4$, before continuing its rotation due to the effect of inertia until t_0+T.

A comparison between the measured results for oil boom model M2 and the modeled results of sway, heave, roll and trajectory of the centroid of the floating boom is shown in Fig.5. As can be seen, good agreements are obtained despite the slight underestimation of the trough and overestimation at its peak, and a slight phase lag also exists between the modeled and measured results of both the sway and roll motions (Figs.5 (c) and (d), respectively) at some phases. These discrepancies may be attributed to the error of the predicted water pressure exerted on the thin boom skirt via the FAVOR technique. As shown in Fig.5(d), the oil boom returns after one wave cycle to the initial position due to the constraint of the mooring lines. Furthermore, the overall moving trend predicted by the numerical model is consistent with the measured one, except at the moments when the boom approaches its furthest positions.

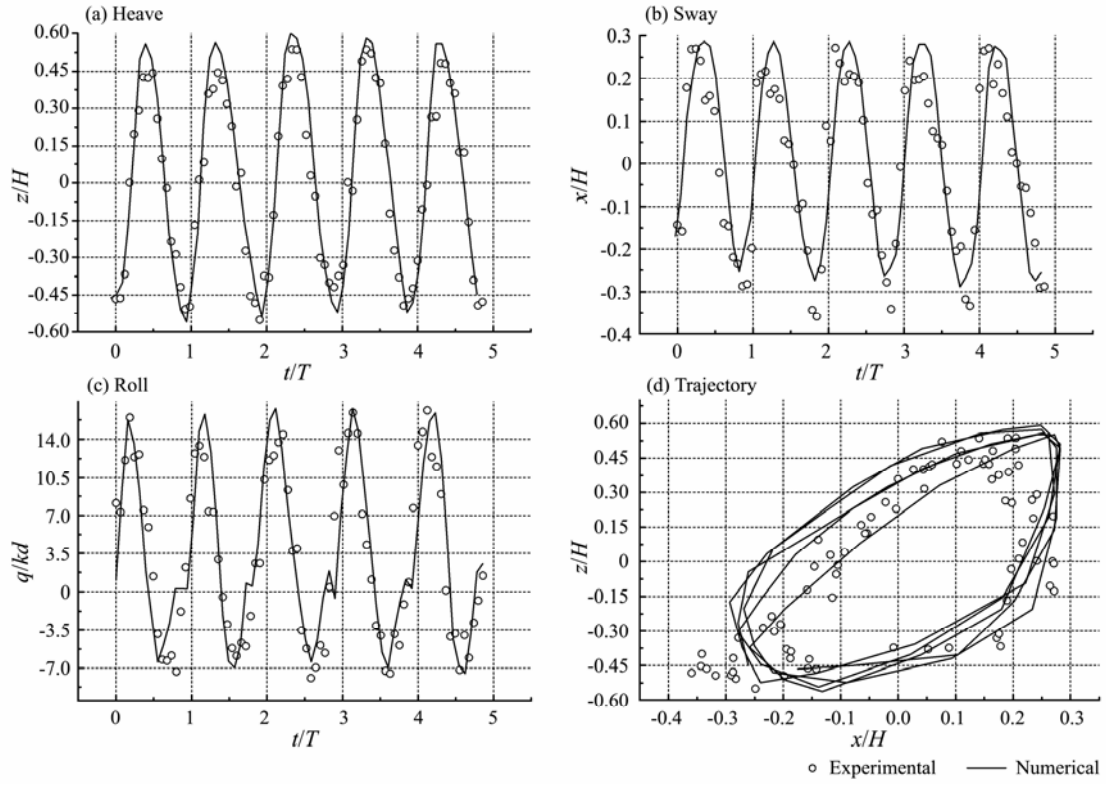

Fig.5 Comparison of measured and modeled results of the motions of oil boom under regular wave.

4 Simulations of Flow Fields and Motion Responses of Different Floating Boom Models

4.1 Comparison Between Movable and Fixed Floating Booms

The floating boom model M2 is taken as an example in comparing the boom restrained by the two mooring lines and the one that is completely fixed. Wave height and wave period were set at 0.04 m and 1.3 s, respectively, and a constant current with velocity of 0.139 m s^{-1} and uniform distribution in the vertical direction was imposed at the right-side boundary. The motion of the floating boom depends on the inertia of the floating boom and the interaction of the combined wave-current. As shown in Fig.6, vortex shedding around the tip of the boom skirt is well reproduced by the present model. Flow velocity is much more severely disturbed by the fixed floating boom than by the movable boom, thus making the vorticity around the fixed boom much more intensive. Furthermore, the vorticity expands much further downward than those around the movable boom. Although water level difference is remarkable between the two sides of the fixed boom, this is almost invisible for the movable boom. Such differences suggest the absolute necessity of using a movable floating boom in assessing the hydraulic performances of the floating booms.

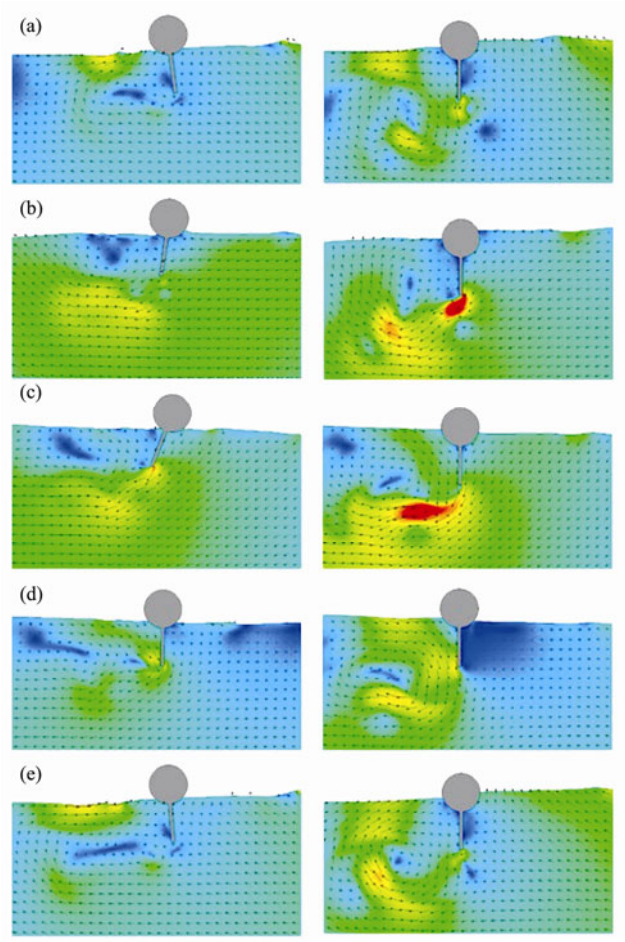

Fig.6 Modeled results of the snapshots of velocity field and oil boom pose under wave with $H=0.04$ m, $T=1.3$ s. a), $t=t_0$; b), $t=t_0+T/4$; c) $t=t_0+T/2$; d), $t=t_0+3T/4$; and e), $t=t_0+T$. Left: movable floating boom; Right: fixed floating boom.

4.2 Indication of the Containment Failure Using Tracers

Tracers are uniformly released along a vertical line at x = 0.7 m and ranging from z = 0.66 m to 0.78 m on the upstream of the boom, to investigate the containment failure mechanism of oil boom. The round tracers are expected to simulate the movement of oil droplets, which have a diameter of 0.002 m and a density of $\rho = 950\,\mathrm{kg\,m^{-3}}$. There exists a single vortex region for the case of the movable floating boom and two regions for the fixed boom. Interestingly, the tracers can also be separated into two groups as they pass below the tip of the boom skirt (Fig.7). One group moves with vortex behind the boom (or in front of the boom if it is fixed), and another moves toward the downstream direction with flow. When the tracers of the second group pass below the boom, they first go downward with the flow and then go upward to the free surface due to buoyancy with oscillation. This group of tracers completely escapes from containment in the boom, and this is considered containment failure.

Meanwhile, the tracers of the first group are trapped by the vortices. Although they have escaped from the boom, they may not be considered as failure containment because they may still follow up with the boom for a long period of time. Oil droplets are more susceptible to the waves in the area ahead of the floating boom, and the down flows before the boom and the rising flow after the boom. This area is called fluctuation area. Comparing the particle trajectory for the conditions of the movable and the fixed floating booms, we can see that more tracers could be trapped by the fixed floating boom than by the movable one.

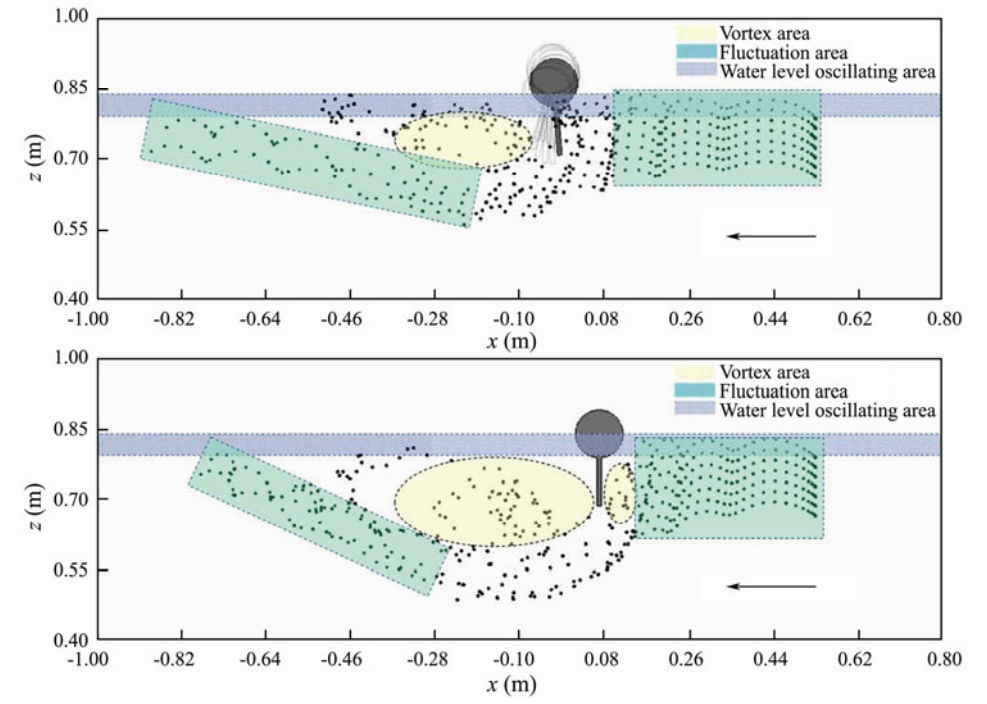

Fig.7 Modeled results of the Lagrangian particle field of the oil boom for $H=0.04$ m, $T=1.3$ s. Top, movable floating boom; Bottom, fixed floating boom.

4.3 Effects of Boom Parameters on Effective Draft and Freeboard

The freeboard and effective draft of the floating boom play key functions in preventing containment failures, such splash-over and drainage. As shown in Fig.8, due to the composite action of the water pressure and the pulling force of the mooring lines, the effective drafts of the floating booms decrease with increasing current velocity for both two models. As for the effective freeboard, the current has positive effects on lighter floating boom, but negative ones on the heavier floating boom. This result can be attributed to the heavier booms having smaller roll responses, thus generating larger drag velocity around the boom, which leads to larger draft due to the suction effect. The effect of the wave can be examined directly by comparing the effective freeboard and draft in various wave conditions. Results indicate that the effective freeboard and draft are directly proportional to the wave steepness. Increased wave height can have a negative effect on the boom effectiveness, especially if the wave steepness is fixed.

As shown in Fig.9, the simulated results of the effective draft for floating booms with different skirt lengths decrease in the same way as the current velocity increases, whereas those for the effective freeboard are positively related to the current velocity. The effect of the current is less pronounced on the shorter skirt models than on the longer skirt models, that is, the longer skirt, the larger pressed area of flow water. Thus, the modeled effective draft and freeboard of the boom model with longer skirt tend to follow with the flow more closely. As shown in Fig.10, the modeled effective draft for floating booms with different floater diameter decreases as the current velocity increases. However, the effective freeboard is not much affected by the floater diameter.

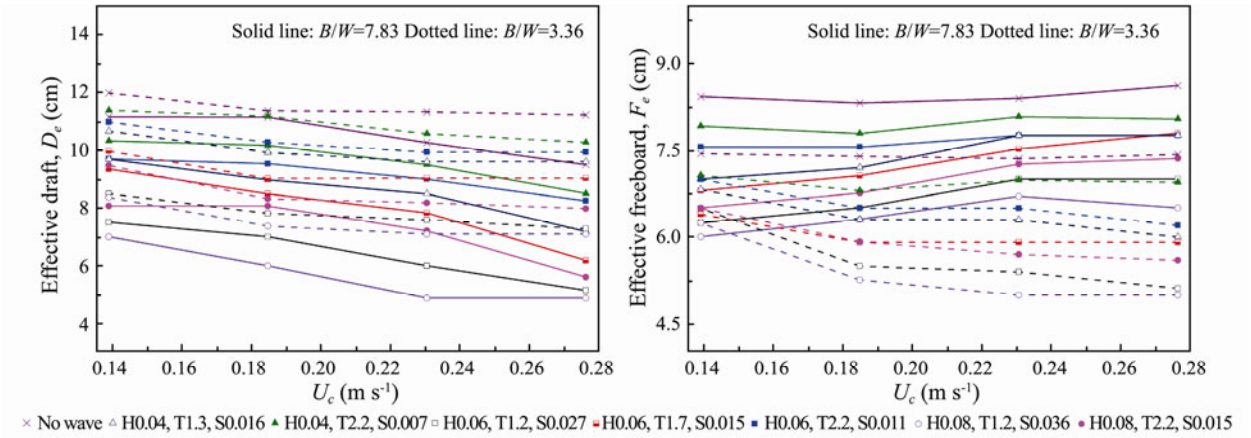

Fig.8 Simulated results of boom effectiveness versus current velocity U_c subject to various conditions of waves for boom models M1 and M3 with B/W ratios of 7.83 and 3.36, respectively. Left, effective draft D_e; Right, effective freeboard F_e.

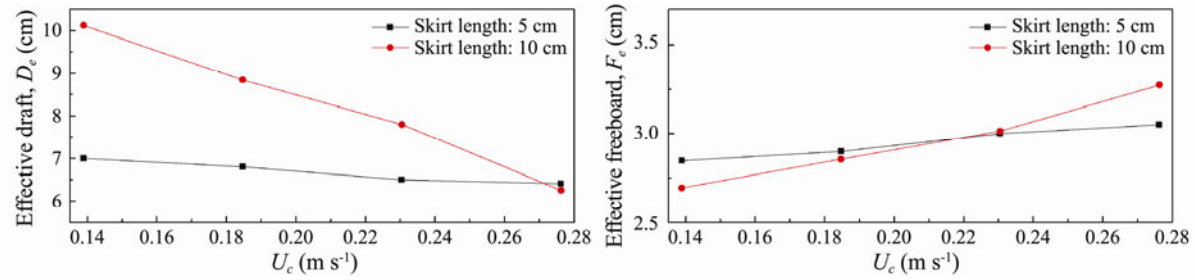

Fig.9 Simulated results of boom effectiveness versus current velocity U_c subject to fixed wave (H=0.04 m, T=2.2 s) for boom models M4 and M5 with B/W ratio about 3.50. Left, effective draft D_e; Right, effective freeboard F_e.

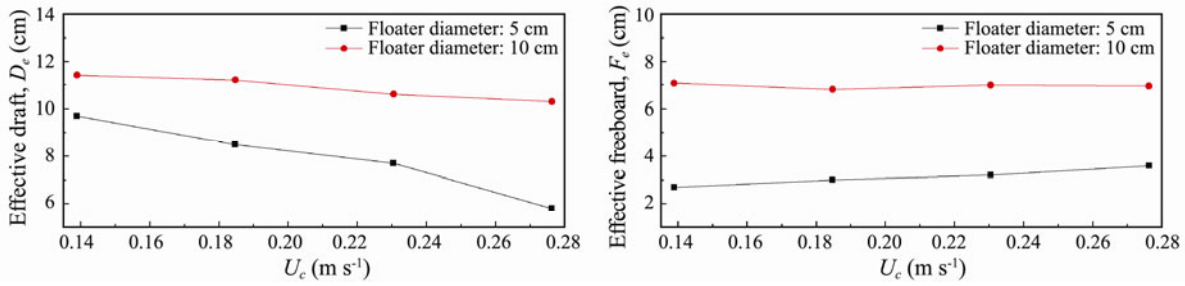

Fig.10 Simulated results of boom effectiveness versus current velocity U_c subject to fixed wave (H=0.04 m, T=2.2 s) for boom models M3 and M4 with B/W ratio about 3.50. Left, effective draft D_e; Right, effective freeboard F_e.

4 Conclusions

A numerical flume is established to investigate the floating boom responses in the wave-current coupling conditions. We then validated the numerical model by conducting experiment tests in terms of floating boom motion responses, including the trajectory. A comparison of the modeled flow field under combined wave and current for movable and fixed floating boom indicates the necessity of utilizing a movable floating boom in performance assessment. Tracer simulations show that oil droplets are either trapped by the vortices in the front or rear of the floating boom or move by escaping following the current via the tip of the skirt. Furthermore, heavier boom has good performance in resisting waves and currents, and is apt to gain a larger effective draft. Finally, numerical simulation implies that the effective draft is significantly affected by the skirt length and the floater diameter, whereas the freeboard is affected by the skirt length.

Acknowledgements

This research is supported by the Foundation for Innovative Research Groups of the National Natural Science Foundation of China (No. 51321065) and the Program of International S&T Cooperation (No. S2015ZR1030).

References

Amini, A., Bollaert, E., Boillat, J. L., and Schleiss, A. J., 2008. Dynamics of low-viscosity oils retained by rigid and flexible barriers. *Ocean Engineering*, **35** (14): 1479-1491.

Amini, A., Mahzari, M., Bollaert, E., and Schleiss, A., 2005. Fluid-structure interaction analysis applied to oil containment booms. *The Proceedings of 19th International Oil Spill Conference*, Florida, USA, 585-588.

Castro, A., Iglesias, G., Carballo, R., and Fraguela, J., 2010. Floating boom performance under waves and currents. *Journal of Hazardous Materials*, **174** (1): 226-235.

Fang, F., and Johnston, A. J., 2001a. Oil containment by boom in waves and wind. I: Numerical model. *Journal of Waterway, Port, Coastal, and Ocean Engineering*, **127** (4): 222-227.

Fang, F., and Johnston, A. J., 2001b. Oil containment by boom in waves and wind. II: Waves. *Journal of Waterway, Port, Coastal, and Ocean Engineering*, **127** (4): 228-233.

Fang, F., and Johnston, A. J., 2001c. Oil containment by boom in waves and wind. III: Containment failure. *Journal of Waterway, Port, Coastal, and Ocean Engineering*, **127** (4): 234-239.

Feng, X., Wu, W. Q., and Wu, W. F., 2011. Numerical simulation technology of oil containment by boom. *Procedia Environmental Sciences*, **8**: 40-47.

Goodman, R., Brown, H., An, C. F., and Rowe, R. D., 1996. Dynamic modelling of oil boom failure using computational fluid dynamics. *Spill Science & Technology Bulletin*, **3** (4): 213-216.

Groeneweg, J., and Battjes, J., 2003. Three-dimensional wave effects on a steady current. *Journal of Fluid Mechanics*, **478**: 325-343.

Hirt, C. W., and Nichols, B. D., 1981. Volume of fluid (VOF) method for the dynamics of free boundaries. *Journal of Computational Physics*, **39** (1): 201-225.

Hirt, C. W., and Sicilian, J. M., 1985. A porosity technique for the definition of obstacles in rectangular cell meshes. The Proceedings of *4th International Conference on Numerical Ship Hydrodynamics*. National Academy of Sicence, Washington, DC.

Iglesias, G., Castro, A., and Fraguela, J., 2010. Artificial intelligence applied to floating boom behavior under waves and currents. *Ocean Engineering*, **37** (17): 1513-1521.

Jacobsen, N. G., Fuhrman, D. R., and Fredsøe, J., 2012. A wave generation toolbox for the open-source cfd library: Openfoam®. *International Journal for Numerical Methods in Fluids*, **70** (9): 1073-1088.

Kim, M., Muralidharan, S., Kee, S., Johnson, R., and Seymour, R., 1998. Seakeeping performance of a containment boom section in random waves and currents. *Ocean Engineering*, **25** (2): 143-172.

Klopman, G., 1994. Vertical structure of the flow due to waves and currents, part 2: Laser-doppler flow measurements for waves following or opposing a current. *The Progress Report of Delft Hydraulics*, The Netherlands, No. H840.32.

Lee, C., and Kang, K., 1995. Development of optimum oil fences in currents and waves. *Annual Report of Advanced Fluids Engineering Research Center*, **7**-41.

Shi, Y., Li, S. W., and Zhang, H. Q., 2017. Experimental studies on performances of flexible floating oil boom under coupled wave-current. *Applied Ocean Research* (Accepted).

Yang, X., and Liu, M., 2013. Numerical modeling of oil spill containment by boom using sph. *Science China Physics, Mechanics and Astronomy*, **56** (2): 315-321.

(Edited by Xie Jun)